Molecular dynamics simulation of fractal aggregate diffusion

Gaurav Pranami, Monica H. Lamm,* and R. Dennis Vigil†
Department of Chemical and Biological Engineering, Iowa State University, Ames, Iowa 50011, USA
(Received 15 July 2009; revised manuscript received 28 May 2010; published 12 November 2010)

The diffusion of fractal aggregates constructed with the method by Thouy and Jullien [J. Phys. A **27**, 2953 (1994)] comprised of N_p spherical primary particles was studied as a function of the aggregate mass and fractal dimension using molecular dynamics simulations. It is shown that finite-size effects have a strong impact on the apparent value of the diffusion coefficient (D), but these can be corrected by carrying out simulations using different simulation box sizes. Specifically, the diffusion coefficient is inversely proportional to the length of a cubic simulation box, and the constant of proportionality appears to be independent of the aggregate mass and fractal dimension. Using this result, it is possible to compute infinite dilution diffusion coefficients (D_o) for aggregates of arbitrary size and fractal dimension, and it was found that $D_o \propto N_p^{-1/d_f}$, as is often assumed by investigators simulating Brownian aggregation of fractal aggregates. The ratio of hydrodynamic radius to radius of gyration is computed and shown to be independent of mass for aggregates of fixed fractal dimension, thus enabling an estimate of the diffusion coefficient for a fractal aggregate based on its radius of gyration.

DOI: 10.1103/PhysRevE.82.051402 PACS number(s): 61.43.Hv

I. INTRODUCTION

The formation of fractal clusters due to aggregation of compact spherical primary particles is an important process that occurs in many physical situations, such as during the synthesis of particulate material in aerosol and colloidal reactors. Because the resulting particle morphology and size distribution can have a strong impact on product quality, for example, in biomedical drug delivery applications that may require specific particle size and shape [1–3], it is necessary to develop accurate models of particle aggregation for the purposes of prediction and control. At the reactor scale, these models are usually formulated in terms of population balance equations, which are simply statements of continuity for the density of particles with specific properties. For example, in a closed system undergoing irreversible aggregation, the particle size distribution is governed by the Smoluchowski equation,

$$\frac{dc_k}{dt} = \frac{1}{2}\sum_{i+j=k} K_{ij}c_i c_j - c_k\sum_{j=1}^{\infty} K_{kj}c_j, \tag{1}$$

where c_k is the concentration of aggregates containing k primary particles (k-mer) and the aggregation kernel K_{ij} is a symmetric matrix of rate constants describing reactions between i-mers and j-mers.

The functional form for K_{ij} depends upon many microscopic details of aggregation events including the transport mechanism responsible for particle collisions, the collision efficiency (fraction of collisions that lead to an aggregation event), and particle morphology. In some cases K_{ij} can be derived analytically by invoking simplifying assumptions and applying physical reasoning. A particularly important example is the case of particles undergoing diffusion-limited aggregation under the influence of Brownian motion, which includes colloidal dispersions of particles that are too small to be influenced by fluid shear, as in the case of nanoparticles. The relevant Brownian kernel, first derived by Smoluchowski [4,5], is given by

$$K_{ij} = 4\pi[R_i + R_j][D_i + D_j], \tag{2}$$

where the sum of the radii R_i+R_j represents the effective collision cross-sectional radius and D_i is the diffusion coefficient of an i-mer. It follows from Eq. (2), that in order to express K_{ij} explicitly in terms of i and j, the dependencies of R_i and D_i on the particle mass i must be known. For compact spherical aggregates, these relations can be obtained from simple geometrical considerations and by invoking the Stokes-Einstein relation so that

$$R_i = \left(\frac{3i}{4\pi\rho_p}\right)^{1/3} \tag{3}$$

and

$$D_i = \frac{k_b T}{6\pi\eta R_i}, \tag{4}$$

where ρ_p is the particle density and η is the viscosity of the suspending fluid.

Many processes, however, result in aggregates with non-Euclidean size scaling and they therefore cannot be described by Eqs. (3) and (4). For example, in the absence of cluster restructuring, particles produced by diffusion-limited aggregation (DLA) possess ramified morphology characterized by a low mass fractal dimension $d_f \sim 1.8$, where d_f is defined by $i \propto (R_g)^{d_f}$ [6,7]. Here, i is the number of primary particles in the aggregate and R_g is the radius of gyration of the cluster. Reaction-limited aggregation (RLA) produces more compact aggregates ($d_f \sim 2.1$) [6,8], but even these clusters are significantly different than spheres and therefore may not obey Eqs. (3) and (4).

The most straightforward and commonly used method for generalizing the Brownian kernel to include nonspherical fractal aggregates is to assume that the appropriate particle

*Corresponding author; mhlamm@iastate.edu
†Corresponding author; vigil@iastate.edu

TABLE I. The ratio of the hydrodynamic radius to the radius of gyration ($R_h/R_g=\beta$) of fractal aggregates in the continuum regime measured using light scattering (SLS/DLS) as reported in the literature.

Author	Primary particle	Size (nm)	d_f	β
Lin *et al.* [7]	Gold	7.5	1.85	0.93
	Silica	3.5		
	Polystyrene	19		
Wang *et al.* [12]	Polystyrene	28	1.75	0.71 ± 0.05
Kaetzel *et al.* [16]	Pyrogenic silica		1.5–1.85	0.79–0.99
Wiltzius [17]	Silica	50–700	2.1	0.72 ± 0.02
				0.83[a]
Lin *et al.* [8]	Gold	7.5	2.1	1.0
	Silica	3.5		
	Polystyrene	19		
Wang *et al.* [12]	Polystyrene	28	2.15	0.97 ± 0.05

[a]As corrected by Wang *et al.* [12].

radius to be used in Eqs. (2) and (4) can be obtained directly from the fractal dimension (i.e., $R_i \approx R_g \propto i^{1/d_f}$). This assumption has been proven valid for a polymer chain in good solvent ($d_f=1.7$) by molecular dynamics (MD) simulations of single polymer chain in a bath of solvent particles [9]. Taking hydrodynamic interactions into account the Zimm model predicts the scaling relationship for the diffusion coefficient for a polymer in good solvent at infinite dilution to be $D \propto R_g^{-1} \propto N_{\mathrm{mon}}^{-1/d_f}$, where N_{mon} is the number of monomers in the polymer chain. Under the conditions of good solvent, the polymer chain stretches out and effectively moves as a solid particle [10], which analogous to the behavior of a fractal aggregate with open morphology. With the exception of a polymer chain in good solvent, the validity of the assumption $R_i \approx R_g \propto i^{1/d_f}$ has not been rigorously established for a range of fractal dimensions. Substantial conflicting information derived from experimental, theoretical, and molecular simulations has been reported concerning the dependence of the diffusion coefficient on the radius of gyration for fractal aggregates. Furthermore, the relationship between R_g and the hydrodynamic radius, R_h (radius of a sphere with equivalent mobility) is also not well understood for fractal aggregates.

The systematic experimental measurement of the diffusion coefficient for fractal aggregates using methods such as dynamic light scattering, settling velocity, and differential electrophoretic mobility analysis, is a challenging problem [11]. For example, an inherent difficulty with any experiment is the near impossibility of obtaining homogeneous samples of aggregates with specific mass and fractal dimension at the desired solvent density. Consequently, experimental measurements are convoluted by the existence of a distribution of aggregate sizes and shapes, and this polydispersity must be taken into account while interpreting the data by either determining these distributions independently or by assuming a distribution [12,13]. It is also nontrivial to decouple contributions from translational and rotational diffusion components to the measured diffusivity [14,15]. Despite these difficulties, it has been demonstrated that in the continuum regime the ratio R_h/R_g approaches a fixed value, β, for aggregates containing sufficiently large numbers of primary particles [7,8,12,16,17]. However, the values of β reported by various investigators can vary widely, as illustrated by the results summarized in Table I. Specifically, the values reported for β range between 0.71–0.93 for DLA aggregates and 0.83–1.0 for RLA aggregates.

Theoretical models for predicting diffusion coefficients have also been developed by approximating the fractal aggregates as porous objects [18–20]. In these models, the fluid motion on the outside of an aggregate is modeled using Stokes' equation and inside the pores with Brinkman's equation. The R_h/R_g predicted by these models is, in general, greater than the experimental measurements and the predictions from models based on Kirkwood-Riseman hydrodynamic theory [21]. The results from models based on Kirkwood-Riseman theory generally agree well with experiments [11,22–24]. However, there are some exceptions as summarized in Table II, where the theoretical predictions for the value of β can be up to an order of magnitude greater than experimentally measured values. Clearly, it is important to address the inconsistencies in the observed experimental and theoretical values for R_h/R_g reported in the literature.

Particle-based molecular simulations offer a promising route to systematically study fractal aggregate diffusion because practical difficulties associated with carrying out experiments and some simplifying assumptions associated with purely theoretical models can be avoided. Recently Moskal *et al.* [26] employed Brownian dynamics (BD) to obtain the diffusion coefficient of aerosol particle aggregates in the continuum regime. Their simulations consisted of 100 aggregates (with normally distributed fractal dimensions) containing 100 primary particles each. The BD trajectories thus generated were used to evaluate mean diffusivity as a function of mean fractal dimension d_f and size N. The diffusivities obtained from these BD simulations are consistently smaller than diffusion coefficients predicted by theories using equivalent radii methods. However, because BD simulation is an implicit solvent method and it therefore requires as an *input* the solute mobility, the usefulness of BD simula-

TABLE II. The ratio of the hydrodynamic radius to the radius of gyration ($R_h/R_g=\beta$) of fractal aggregates in the continuum regime derived from theoretical models as reported in the literature. KR: Kirkwood-Riseman hydrodynamic theory. SB: aggregates modeled as porous bodies, and flow inside and outside the pores is modeled using the Stokes and Brinkman equations. G: general solution of Stokes equation.

Author	Method	Aggregate model	d_f	β
Hess *et al.* [23]	KR	Spherically symmetric fractal; Number density, $c(r)=Ar^{-\beta}$	1.8	1.29
			2.1	1.46
Chen *et al.* [22]	KR	Off-lattice cluster-cluster aggregates	1.8	0.875
			2.1	0.97
Rogak *et al.* [24]	KR	Self-similar aggregates with uniform porosity	1.79	0.89
			2.1	1.0
Lattuada *et al.* [11]	KR	Uses radial distribution function of an aggregate	1.86	0.765
			2.05	0.831
van Saarloos [18]	SB	Porous sphere model of Debye Bueche		1.23
Tandon *et al.* [19]	SB	Radially uniform and spherically porous aggregate	2.3	R_h is 20% larger than [22]
Veerapaneni *et al.* [20]	SB	Constant volume averaged porosity	2.1	1.03
Filippov *et al.* [25]	G	Numerically generated fractal aggregates with specified pre-factor	1.8	0.9–1.0

tions for computing diffusivities is questionable. Furthermore, BD simulations do not conserve momentum transport through the solvent phase, and therefore they do not correctly account for hydrodynamic interactions. Therefore, diffusion coefficients obtained using BD are useful only for qualitative comparison.

In contrast, MD simulations directly account for solute-solvent interactions because solvent molecules are represented explicitly, and hence the diffusion coefficients obtained can be expected to be more accurate. However, because MD simulations include an explicit solvent, simulation of large aggregates or populations of aggregates can become computationally intractable. Although no MD simulations of fractal aggregates have been reported, Heyes *et al.* [27–31] have used MD simulations to study translational and rotational diffusion of spherical clusters using purely repulsive pair potentials, and it was found that the difference in the translational diffusivity of rigid and dynamic clusters was statistically negligible [27]. It was also shown that both the translational and rotational diffusivities increased with increasing simulation box size [27], which is a manifestation of finite size effects. At high solvent densities of 0.8–0.9 (reduced units) both the translational diffusivity and rotational diffusivity were found to be independent of the mass ratio of the cluster primary particle and solvent particle [28,29]. The translational and rotational diffusivities decreased with increasing solvent density and cluster size [29]. As the solvent density was increased, the reorientation relaxation time also increased [29]. However, these simulations were run using an *ad hoc* velocity rescaling technique to thermostat the system, which can introduce deviations in the system dynamics. Additionally, the results were not properly corrected for finite-size effects, and simulations were performed only for dense spherical clusters.

In this work we compute the diffusivity (D) of nanoparticle aggregates in the limit of infinite dilution as a function of their size (N_p) and fractal dimension (d_f) using MD simulations in the presence of explicit solvent molecules in the continuum regime. We find that D scales as N_p^{-1/d_f} and that the ratio of hydrodynamic radius to the radius of gyration attains a fixed value, β, for sufficiently large aggregate size. The resulting values of β for fractal dimensions of 1.8 and 2.5 are found to be 0.76 and 0.98, respectively. These results are then compared with corresponding values based on experiments and hydrodynamic theory reported in the literature.

II. COMPUTATIONAL DETAILS

A. Generation of fractal aggregates

Off-lattice fractal aggregates with precisely controlled mass and fractal dimension were generated using the recipe proposed by Thouy and Jullien [32,33]. In the first step of this hierarchical method, $2N$ monomers (primary particles) are paired to form N dimers. Similarly, in the second step the N dimers are paired to form $N/2$ tetramers and so on, until a single aggregate with $2N$ primary particles remains. At each

step of the cluster pairing process, the clusters are connected and oriented so that the resulting aggregate maintains the desired fractal dimension. Even within the constraint of constant fractal dimension there are several degrees of freedom in combining two clusters, so the process is carried out stochastically. Hence, it is possible to generate a large number of unique fractal aggregates with specific size and fractal dimension, and the number of such isomers increases rapidly with increasing cluster size.

There are other well-known methods for producing fractal aggregates. The Thouy and Jullien algorithm was selected for generating the aggregates because this study requires a set of independent fractal aggregates with fixed mass and fixed fractal dimension. Other approaches for generating fractal clusters, such as DLA or cluster-cluster aggregation (CCA), are impractical because numerous simulations would be required just to generate a set of clusters with the desired masses. Moreover, even after a sufficient number of clusters with the desired masses are produced, the variance in the internal fractal dimensions of these clusters will be quite large because methods such as DLA and CCA only assure that a very large ensemble of clusters with different masses satisfy fractal scaling. In other words, DLA, CCA, and other well-known methods for generating fractal aggregates do not provide any control over the internal fractal dimension of individual aggregates and would consequently introduce much greater uncertainty and variability in the cluster characteristics. The advantage of the Thouy and Jullien construction is that it generates clusters for any prescribed fractal dimension and satisfies the scaling relation exactly (not just in the sense of an ensemble of particles, but in terms of the internal fractal dimension) at each cumulative internal mass of $2^p \times M$, where M is the mass of a single monomer and p is an integer. It is true that the scaling may not be satisfied exactly at intermediate values of the cumulative internal mass, but it is difficult to envision how any significant deviation could be introduced while still satisfying the scaling at every generation p. Hence, the Thouy and Jullien construction was chosen as it is the only known method for constructing fractal clusters that provides a significant measure of control over the internal fractal dimension of the resulting aggregates.

In order to verify that the aggregates produced by using the Thouy and Jullien methodology have the desired fractal dimension, we generated six aggregates of sizes $N=\{32,64,128,256,512,1024\}$ corresponding to each of the fractal dimensions $d_f=\{1.8,2.5\}$. The radius of gyration for each cluster was calculated as

$$R_g^2 = \frac{1}{N}\sum_{i=1}^{N}(r_i - r_{\mathrm{cm}})^2, \tag{5}$$

where r_i is the position of particle i and r_{cm} is the position of the cluster center of mass. As expected, a plot of $\ln(N)$ vs $\ln(R_g)$ for these clusters yields straight line fits with slopes 1.8 and 2.5, as shown in Fig. 1. Two dimensional projections for two fractal clusters (each of size $N=256$) with fractal dimensions $d_f=1.8$ and 2.5 produced using the method of Thouy and Jullien are shown in Fig. 2.

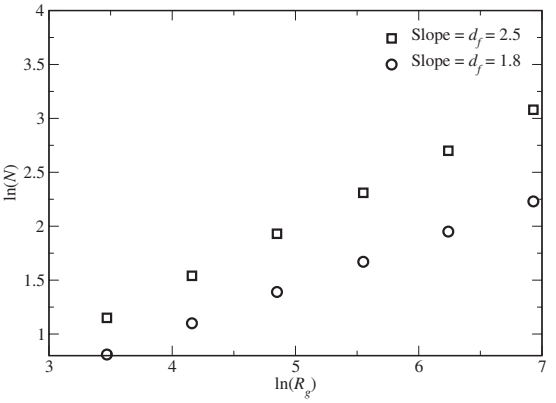

FIG. 1. Plot of N versus R_g for clusters of fractal dimensions 1.8 and 2.5 generated using the hierarchical method of Thouy and Jullien [32,33]. The straight line fits through the data yield the slopes 1.8 and 2.5, thereby validating this method for generating fractal aggregates of precisely controlled N and d_f.

Fractal dimension alone is insufficient to uniquely characterize aggregate morphology. For example, different measured values of the internal fractal dimension for any model aggregate, regardless of how it was constructed can be obtained depending upon whether the measured mass scaling is carried out in concentric spheres, long cylinders, rectangular boxes, or ellipsoids with various aspect ratios. Therefore, to further characterize the aggregates generated using the method of Thouy and Jullien, we calculated the shape anisotropy parameters [34], A_{13} and A_{23}, where

$$A_{13} = I_1/I_3, \tag{6}$$

$$A_{23} = I_2/I_3, \tag{7}$$

and I_1, I_2, and I_3 are the principle moments of inertia of the aggregate with $I_1 > I_2 > I_3$. For each fractal dimension studied, we generated 1000 fractal aggregates for all cluster

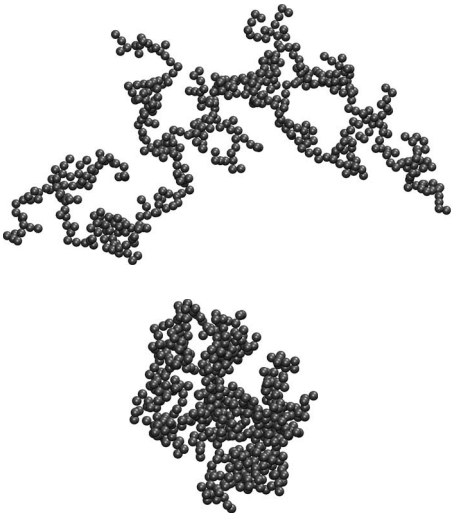

FIG. 2. Two-dimensional projections of fractal clusters generated using the hierarchical method of Thouy and Jullien [32,33]. $N=256$, $d_f=1.8$ (top); $N=256$, $d_f=2.5$ (bottom).

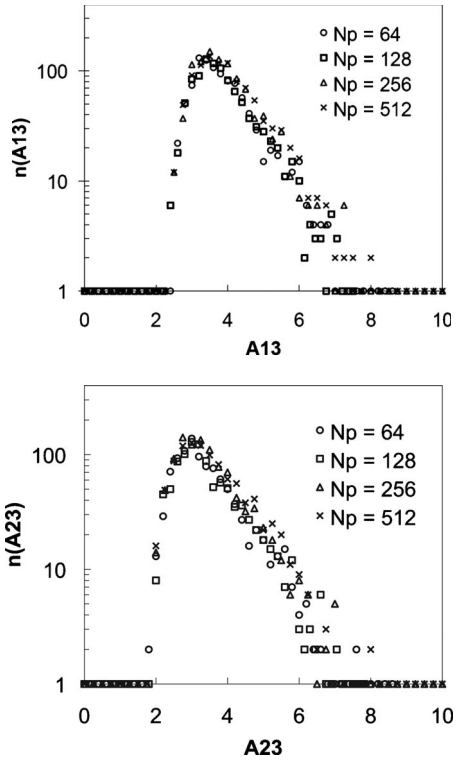

FIG. 3. Frequency distributions of A_{13} and A_{23} for fractal aggregates clusters generated using the hierarchical method of Thouy and Jullien [32,33].

sizes, with the exception of cluster size 512 and fractal dimension d_f=2.5 where we generated 100 fractal aggregates because of the computational time demands. Frequency distributions for A_{13} and A_{23} were computed for each aggregate cluster size and fractal dimension combination. Figure 3 shows the distributions obtained for A_{13} and A_{23} at a fractal dimension d_f=1.8. Frequency distributions for the other fractal dimensions studied are provided in the supplementary material [35]. These distributions compare favorably with the anisotropy parameter distributions reported by Fry *et al.* [34] for fractal clusters formed in dilute-limit, diffusion-limited cluster-cluster aggregation (DLCA) simulations. From this analysis, it is reasonable to expect that diffusion behavior observed for the Thouy and Jullien aggregates studied here would also be observed for model aggregates generated by other means, such as DLCA simulations. We emphasize here that the advantage of the Thouy and Jullien construction is that unique aggregates with a precise fractal dimension and mass are generated.

B. Simulation details

In MD simulations a system consisting of a collection of particles (which may represent atoms, molecules, or larger entities) is evolved in time by solving the equations of motion for each particle:

$$m\ddot{\vec{r}}_i = \vec{F}_i. \tag{8}$$

Here $\vec{F}_i$ is the net force acting on particle i, which depends on the relative positions of all other particles with respect to particle i, and $\ddot{\vec{r}}_i$ is the second derivative of the position ($\vec{r}_i$) of atom i of mass m with respect to time. Therefore, by neglecting multibody interactions, the net force on particle i can be obtained by summing the pairwise interactions between that particle and all of the other particles in the system. Usually these forces are expressed in terms of the gradient of the pairwise interaction energy potential U so that the total force acting on a given particle is given by

$$\vec{F}_i = -\sum_{j=1,j\neq i}^{n} \nabla U(|\vec{r}_i - \vec{r}_j|). \tag{9}$$

In the above expression n is the total number of particles in the system and $|\vec{r}_i - \vec{r}_j|$ is the distance separating particles i and j. The result of integrating the equations of motion over small time intervals is a record of the system trajectory (i.e., positions and momenta of all constituent particles). Using this information, a variety of structural, dynamical and thermodynamic properties can then be calculated.

In this work, a system comprised of N_s solvent particles and a single fractal aggregate (consisting of N_p primary particles) residing in a cubic simulation box of length L with periodic boundaries was evolved in time using MD simulation. In all simulations, L was chosen to be at least six times the radius of gyration of the chosen solute cluster. The fractal aggregates were represented in the simulations as rigid bodies. At each time step, the total force and torque on the aggregate is computed as the sum of the forces and torques on the primary particles. The coordinates and velocities of the primary particles in the aggregate are updated so that the aggregate moves and rotates as a single entity. Consequently, it was not necessary to define interaction energy potentials between the primary particles that comprise an aggregate. Interactions between two solvent particles and between solvent particles and fractal aggregate primary particles were modeled using a Lennard-Jones (LJ) potential,

$$U(r) = 4\epsilon\left[\left(\frac{\sigma}{r}\right)^{12} - \left(\frac{\sigma}{r}\right)^{6}\right], \tag{10}$$

where r is the distance separating two particles, σ is the size of the interacting particles (assumed to be equal), and ϵ is the well-depth that characterizes the strength of their attraction.

All simulations were carried out in reduced units, as indicated in Table III, using the LAMMPS molecular dynamics program available from Sandia National Laboratory [36,37].

TABLE III. Reduced units used in the MD simulations.

Dimension	Unit
Length	σ_s
Energy	ϵ_s
Mass	m_s
Temperature	ϵ_s/k_b
Time	$\sigma_s\sqrt{m_s/\epsilon_s}$
Diffusivity	$\sigma_s\sqrt{\epsilon_s/m_s}$
Viscosity	$\sqrt{m_s\epsilon_s}/\sigma_s^2$

As was mentioned previously, the size (σ) and mass (m) of the aggregate primary particles and the solvent particles were chosen to be identical and set to unity, i.e., $\sigma_p=\sigma_s=1$ and $m_p=m_s=1$. To ensure that LJ solvent particles were in the liquid state, the number density of solvent particles (ρ_s) and the temperature (T) were fixed at values of 0.85 and 1.2, respectively [38]. The number of solvent particles was calculated as $N_s=V_s/\rho_s$, where V_s is the difference between the volume of the simulation box and the volume of the primary particles. In all simulations the solvent-solvent and solvent-primary particle interactions were identical, i.e., $\epsilon_{s-s}=\epsilon_{s-p}=1$, and the system was equilibrated in the canonical ensemble (NVT) for 2500 reduced time units using a Nose-Hoover thermostat to ensure that all systems studied were at an identical temperature. After the completion of this initial equilibration, the thermostat was turned off to avoid artificially altering the system dynamics [38]. Subsequently, a production run in the microcanonical ensemble (NVE) was carried out for 50 000 reduced time units, and the resulting trajectories of the fractal aggregates were recorded at an interval of one time unit. A time step of 0.005 was found to be suitable for solving the equations of motion for all systems studied in this work.

The diffusion coefficient of fractal aggregates can be computed from trajectories generated by MD simulation using the Einstein relation [39]

$$D=\frac{1}{6}\lim_{\tau\to\infty}\frac{d}{d\tau}\langle[\vec{r}(\tau)-\vec{r}(0)]^2\rangle, \tag{11}$$

where D is the diffusion coefficient, $\vec{r}(\tau)$ is the cluster position at time τ, $\tau=0$ refers to a time origin, and the operator $\langle\ \rangle$ represents the average over time origins. For particles undergoing diffusion, the mean squared displacement grows linearly with time for sufficiently large values of τ, and therefore D can be obtained from a plot of $\langle[\vec{r}(\tau)-\vec{r}(0)]^2\rangle$ vs τ. Alternatively, the diffusion coefficient can be computed from the aggregate velocity autocorrelation function using the Green-Kubo formula [39],

$$D=\int_0^\infty \frac{d\tau\langle\vec{v}(\tau)\cdot\vec{v}(0)\rangle}{3}, \tag{12}$$

where $\vec{v}(\tau)$ is the velocity at time τ. However, due to uncertainty associated with the behavior of the velocity autocorrelation at long times and inaccuracy in evaluating the integral numerically, the diffusion coefficients reported in this work were obtained using Einstein's relation, i.e., Eq. (11).

C. Finite-size effects

As stated previously, the MD simulations were carried out in periodic boxes with lengths $L\geq 6R_g$. Nevertheless, finite size effects due to long-range hydrodynamic interactions can be expected to be important because they decay as the inverse of distance, which is evident from the $1/r$ dependence of the Oseen tensor. Therefore, the dynamic properties of a finite system modeled with periodic boundary conditions are affected by interactions between the system and its periodic images. Yeh *et al.* [40] and Dunweg *et al.* [9,41] proposed the following correction to account for these finite-size effects on the diffusion coefficient:

$$D_o=D+\frac{\xi k_bT}{6\pi\eta L}. \tag{13}$$

In Eq. (13), D_o is the corrected diffusion coefficient, D is the diffusion coefficient obtained from MD simulation in a periodic box with sides of length L, $\xi=2.837\ 297$ [40,41] (constant), k_b is the Boltzmann constant, T is temperature, and η is the dynamic viscosity of the solvent. This relation has been shown to hold for Lennard-Jones fluids [9,40] and TIP3P water [40]. In addition, Yeh *et al.* [40] showed that the variation in viscosity with changes in L is statistically negligible.

III. RESULTS AND DISCUSSION

A. Characterization of fractal aggregates

Table IV lists the mass (N_p), fractal dimension (d_f), and shape anisotropy parameters (A_{13} and A_{23}) for each fractal aggregate that was simulated. The shape anisotropy values for a given fractal aggregate can be compared to the frequency distribution for the corresponding fractal dimension (Fig. 3 and supplementary information) to assess how well the fractal aggregates selected for simulation represent a typical aggregate for that fractal dimension. None of the simulated aggregates have anisotropy values outside the expected distributions for their corresponding fractal dimension.

B. Finite-size effects for fractal aggregates

Based on Eq. (13), it can be expected that at fixed temperature the constant of proportionality between the diffusion coefficient and the inverse box length is independent of the mass and fractal dimension of the diffusing cluster. However, because this equation was not developed specifically for fractal clusters, it is possible that the slope of the linear fit of D versus L^{-1} data could depend upon N_p and d_f. In order to determine whether or not this is the case, several MD simulations were carried out using various simulation box lengths, aggregate sizes, and fractal dimensions, and the data were plotted as shown in Fig. 4. For each aggregate considered, simulations were carried out using several different box sizes. For each such simulation box, ten multiple independent simulations were carried out by randomly varying the initial velocities assigned to all particles. As expected, it was found that D varies linearly with L^{-1}. In addition, the slope appears to be independent of the aggregate size and fractal dimension. It is also evident from the scatter in the data shown in Fig. 4 that in order to deduce the correct slope (and hence the correct diffusion coefficient), it is crucial to carry out multiple independent simulations. Although it would be desirable to carry out ten multiple independent simulations for several box lengths for every aggregate considered in this work, the computational cost would severely restrict the maximum aggregate size that could be considered because the number of solvent particles required increases as R_g^3. However, in view of the fact that Fig. 4 suggests that a uni-

TABLE IV. List of the systems studied in this work. L is the length of the cubic simulation box and is given in the units of R_g of the corresponding fractal aggregates.

N_p	Cluster No.	d_f	A_{13}	A_{23}	$L(\times R_g)$
64	1	1.8[a]	5.19	4.57	8, 10, 12.5, 15
		2.1	2.37	2.05	8, 10, 12.5, 15
		2.3	2.16	2.08	8, 10, 12.5, 15
		2.5[a]	2.09	1.70	8, 10, 12.5, 15
64	2	1.8[a]	4.31	3.79	8, 10, 12.5, 15
		2.1	2.78	2.25	8, 10, 12.5, 15
		2.3	2.01	1.57	8, 10, 12.5, 15
		2.5[a]	2.70	2.29	8, 10, 12.5, 15
64	3	1.8[a]	3.90	3.34	8, 10, 12.5, 15
		2.1	3.24	2.76	8, 10, 12.5, 15
		2.3	2.45	1.82	8, 10, 12.5, 15
		2.5[a]	2.44	2.30	8, 10, 12.5, 15
64	4	1.8[a]	4.47	3.79	6, 7, 8, 9, 10
		2.1	2.35	1.95	8, 10, 12.5, 15
		2.3	2.12	1.55	8, 10, 12.5, 15
		2.5[a]	2.61	2.39	8, 10, 12.5, 15
64	5	1.8[a]	4.71	4.31	8, 10, 12.5, 15
		2.1	2.97	1.95	8, 10, 12.5, 15
		2.3	2.45	2.08	8, 10, 12.5, 15
		2.5[a]	2.01	1.70	8, 10, 12.5, 15
128	1	1.8[a]	3.57	2.86	6, 7, 8, 9, 10
		2.5	2.15	1.80	7, 8, 10, 12.5
256	1	1.8	5.11	4.71	6, 7, 8, 10
		2.5	1.96	1.66	6, 7, 8, 10
512	1	1.8	3.34	3.14	6, 6.5, 7, 10
		2.5	2.17	1.73	6, 7, 8, 9, 10

[a]Ten multiple independent simulations were conducted for each box size.

versal slope exists for the dependence of the diffusion coefficient on inverse box length, we have made use of this slope to compute diffusion coefficients at infinite dilution for all aggregate sizes and fractal dimensions considered. In particular, for each aggregate a single simulation was conducted for each of the different box sizes listed in Table IV. The diffusion coefficients obtained for each box size were then extrapolated linearly to $L^{-1}=0$ (infinite dilution) using the mean value of the slopes shown in Fig. 4, and the finite-size corrected diffusion coefficient, D_o, was obtained from the mean of these extrapolated values. Alternatively, one can determine the mean diffusion coefficient for multiple independent simulations carried out at a single computationally feasible box size and then extrapolate to infinite dilution using the universal slope.

C. Diffusion coefficient scaling with mass and fractal dimension

Figure 5 illustrates the relationship between the corrected diffusion coefficient and the aggregate mass (N_p) for clusters having fractal dimensions of 1.8 and 2.5. Note that each point on this plot required carrying out numerous simulations using different box sizes in order to correct for finite size effects as was discussed above. As expected, for a given fractal dimension, the diffusivity of the aggregates decreases with increasing mass, and the linearity of the plots suggests a power-law relationship between D_o and N_p. The slopes of the best straight line fits through these data were found to be −0.59 and −0.43 for fractal dimensions 1.8 and 2.5, respectively, and these values compare very well with $-1/d_f$ =−0.56 and −0.40. Hence, it appears that the appropriate scaling relation is given by

$$D_o \propto N_p^{-1/d_f}. \tag{14}$$

Since the intercepts of the straight line fits in Fig. 5 are given by −2.66 and −3.16 for fractal dimensions 1.8 and 2.5, respectively, it can be concluded that the proportionality constant for the relation given by Eq. (14) also depends on the fractal dimension.

Equation (14) shows that as the cluster mass increases, the diffusivity of ramified aggregates with a low fractal dimension decreases more quickly than does the diffusivity of compact clusters with a high fractal dimension. This trend can be explained by the fact that the open structure of low

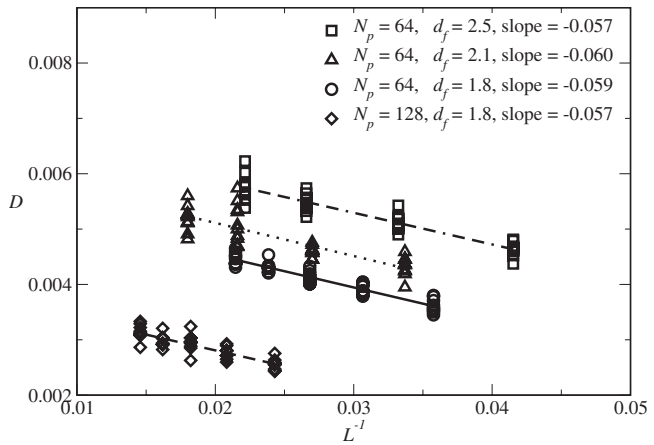

FIG. 4. Variation in the diffusion coefficient (D) of fractal aggregates as a function of the inverse simulation box length (L^{-1}). For an aggregate placed in a box of a given size, ten independent MD simulations were conducted by randomly varying the initial velocity of all particles. The slopes of the least squared straight line fits through the data are indicated in the legend.

fractal dimension clusters provides solvent particles access to nearly all of the primary particles comprising the aggregate, thereby decreasing the Brownian mobility. In contrast, interior primary particles in compact clusters with high d_f are largely shielded from solvent particles.

The dependence of the diffusion coefficient on fractal dimension for fixed aggregate mass (N_p=64) is depicted in Fig. 6. Five unique aggregates were simulated for each of the four fractal dimensions considered (d_f=1.8,2.1,2.3,2.5). It can be seen that for fixed aggregate mass, D_o increases approximately linearly with d_f. Not surprisingly, aggregates with higher values of d_f diffuse faster because the compact morphology results in fewer interactions with solvent particles. The data in Fig. 6 also show significant variation in the diffusivity within clusters that have the same fractal dimension, which suggests that morphological factors other than fractal dimension may be important for predicting the mobility of an aggregate.

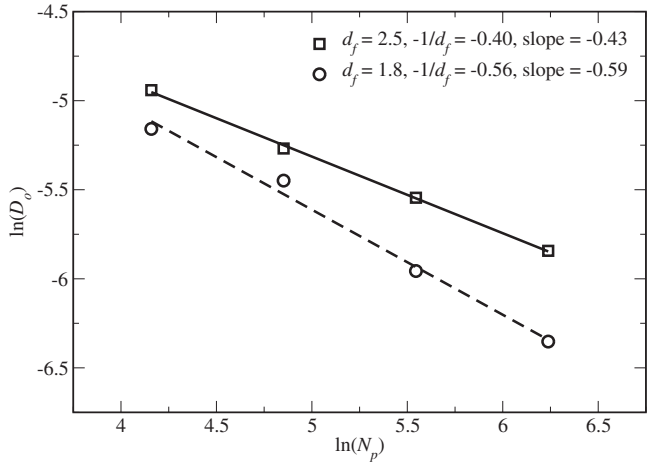

FIG. 5. Variation in the diffusion coefficient (D_o) of aggregates with mass (N_p) and fractal dimension (d_f). The slope of straight line fit through $\ln(D_o)$ vs $\ln(N_p)$ data agrees well with $-1/d_f$ thereby suggesting the scaling relation $D_o \propto N_p^{-1/d_f}$.

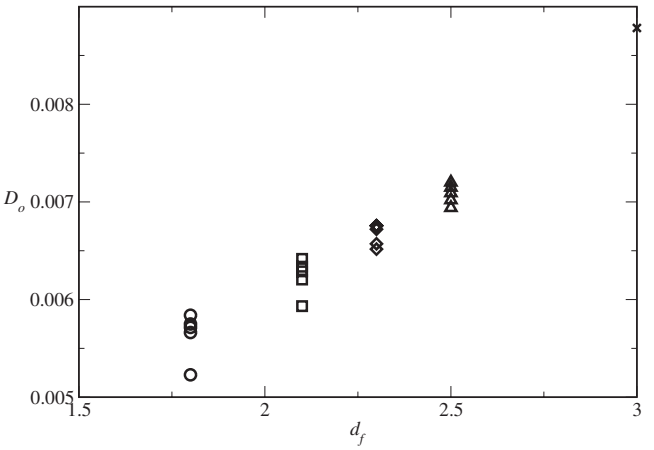

FIG. 6. Variation in the diffusion coefficient with fractal dimension for aggregates containing 64 primary particles. For each fractal dimension considered, five independent aggregates were simulated. The data point indicated by × is the diffusion coefficient of a packed spherical aggregate containing 64 particles as calculated using the Stokes-Einstein relation.

The diffusivity of a spherical aggregate (d_f=3) with mass (N_p=64) was calculated using the Stokes-Einstein formula for a stick boundary condition [42] and this point is also plotted in Fig. 6. It is clear that the location of this point is consistent with an extrapolation of the values of D_o found for the fractal clusters, and therefore it appears that the diffusivity approaches the correct limit as $d_f \rightarrow 3$. In order to obtain the Stokes-Einstein prediction for the spherical aggregate, it was necessary to obtain estimates of the viscosity of the solvent and the hydrodynamic radius of a spherical cluster comprised of 64 spherical primary particles. The viscosity of the solvent (3.12 in reduced units) was inferred using Eq. (13) and the slope reported in Fig. 4. The hydrodynamic radius of the spherical cluster of spherical particles was approximated by the radius of gyration. The latter quantity was obtained by using Monte Carlo simulation to generate an optimally packed spherical aggregate with 64 primary particles. Specifically, the primary particles interacted repulsively according to a Lennard-Jones potential with a cutoff at $2^{1/6}\sigma$, and the spherical aggregate was produced by ramping the pressure to a high value while simultaneously decreasing the temperature.

D. Ratio of hydrodynamic radius to radius of gyration

The hydrodynamic radius R_h of the fractal aggregates was computed using the Stokes-Einstein relation

$$R_h = \frac{k_b T}{6\pi\eta D_o}, \tag{15}$$

and the resulting values for the ratio $\beta = R_h/R_g$ are plotted as a function of aggregate mass in Fig. 7 for clusters with fractal dimensions 1.8 and 2.5. In both cases, within statistical uncertainty β remains constant even for the smallest aggregates comprised of 64 primary particles, and the mean values of β for d_f=1.8 and 2.5 were found to be 0.76 and 0.98, respectively. Our result of β for aggregates of d_f=2.5 agrees

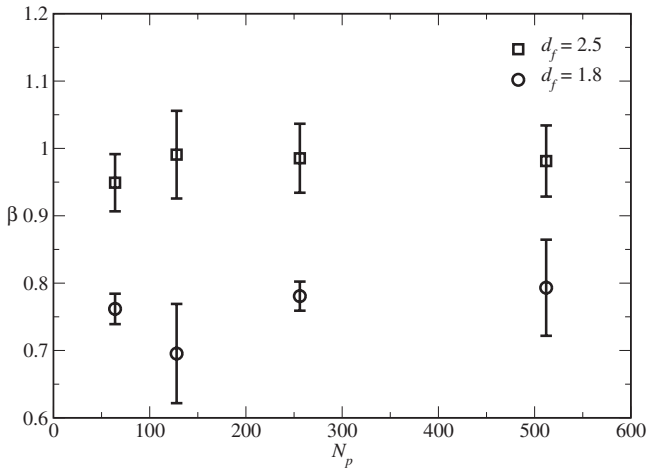

FIG. 7. Ratio of hydrodynamic radius to radius of gyration (β) as a function of the mass of aggregate (N_p) for fractal dimensions (d_f) of 1.8 and 2.5. Within statistical uncertainty β is fixed for a given fractal dimension irrespective of the size of the aggregate. For d_f of 1.8 and 2.5, β is found to be 0.76 and 0.98, respectively.

well with experimental measurements [8,12] and theoretical predictions [20,22,24] reported in the literature for RLA aggregates. The value of β obtained for aggregates formed in the DLA regime (d_f=1.8) also agrees with previous experimentally determined [12] and theoretically derived [11] values. However, these results should be interpreted with the understanding that in this work there is no size separation between the solvent and solute primary particles. Thus, we are in effect coarse-graining the solvent since in real systems the solvent molecules are much smaller than the primary solute particles. Because of this coarse-grained representation of the solvent, the magnitude of the fluctuations in the net force exerted by solvent particles on solute particles can be expected to be larger than if the solvent were represented by an enormous number of much smaller molecules surrounding solute particles. Hence, a likely consequence of coarse-graining the solvent is an overestimation of the diffusion coefficients for solute clusters, which, in turn, underpredicts the hydrodynamic radius.

IV. CONCLUSIONS

In this work MD simulations were used to study the diffusion of Thouy and Jullien fractal aggregates as a function of their mass and fractal dimension. Because aggregates with carefully controlled mass and fractal dimensions were generated, it was possible to compute diffusion coefficients without having to perform difficult deconvolutions associated with data obtained from experiments, which by necessity employ polydisperse samples of aggregates. Moreover, because solvent particles were represented explicitly, hydrodynamics effects are computed directly and therefore there is no need to invoke simplifying assumptions that are associated with purely theoretical approaches.

The diffusion coefficient of a fractal aggregate has been found to vary linearly with the inverse of the simulation box length (L). Therefore, the intercept of a plot of D vs L^{-1} is the diffusion coefficient corrected for finite size effects (infinite dilution limit). However, it was shown that multiple independent simulations for each simulation box size are required in order to correctly compute this value. Nevertheless, it appears that at constant temperature, the slope of a plot of D vs L^{-1} is independent of the aggregate mass and fractal dimension, and therefore multiple independent simulations need not be performed for every aggregate size and fractal dimension considered.

The infinite dilution diffusion coefficient was also found to scale with aggregate mass according to $D_o \propto N^{-1/d_f}$, which validates an assumption commonly invoked to compute aggregation rate kernels for Brownian aggregation. The ratio of hydrodynamic radius to radius of gyration (R_h/R_g) of fractal aggregates sheds light on dynamic properties and can be measured experimentally. Consequently, R_h/R_g for fractal aggregates has been investigated extensively both theoretically and experimentally in the literature. Unfortunately, there is significant ambiguity in the dependence of R_h/R_g on N_p and d_f in the results reported. In this work, we have shown that R_h/R_g approaches a constant value (β) for even relatively small aggregates of fixed fractal dimension. The value of β for fractal dimensions of 1.8 and 2.5 was found to be 0.76 and 0.98, respectively, which is in good agreement with the experiments conducted by Wang *et al.* [12]

It has been established in the literature that experimentally measured diffusion coefficients of fractal aggregates are convoluted by rotational diffusion. We are currently working on understanding the coupling of rotational and translational diffusion. The diffusion of fractal aggregates also depends on whether the primary particles comprising the aggregates are solvophilic or solvophobic, which in turn governs the aggregation kinetics. This aspect of the diffusion of fractal aggregates has not yet been addressed systematically, and simulations are underway to explore how the diffusion of fractal aggregates varies as the interactions between the aggregate and solvent particles are changed.

ACKNOWLEDGMENTS

The authors acknowledge financial support from the National Science Foundation (Grant No. NIRT-0403864) and helpful discussions with Professor Rodney Fox and Dr. Rastko Sknepnek. Simulations for the aggregate with fractal dimension of 2.1 were completed by Christopher B. Renner, an REU intern supported by National Science Foundation Grant No. EEC-0851519.

[1] B. D. Chithrani, A. A. Ghazani, and W. C. W. Chan, Nano Lett. **6**, 662 (2006).
[2] W. Shi, J. Wang, X. Fan, and H. Gao, Phys. Rev. E **78**, 061914 (2008).
[3] P. K. Jain, K. S. Lee, I. H. El-Sayed, and M. A. El-Sayed, J. Phys. Chem. B **110**, 7238 (2006).
[4] M. Smoluchowski, Phys. Z. **17**, 557 (1916).
[5] M. Smoluchowski, Z. Phys. Chem. **92**, 129 (1917).
[6] R. Botet and R. Jullien, *Aggregation and Fractal Aggregates* (World Scientific, Singapore, 1987).
[7] M. Y. Lin, H. M. Lindsay, D. A. Weitz, R. Klein, R. C. Ball, and P. Meakin, J. Phys.: Condens. Matter **2**, 3093 (1990).
[8] M. Y. Lin, H. M. Lindsay, D. A. Weitz, R. C. Ball, R. Klein, and P. Meakin, Phys. Rev. A **41**, 2005 (1990).
[9] B. Dünweg and K. Kremer, J. Chem. Phys. **99**, 6983 (1993).
[10] M. Rubenstein and R. H. Colby, *Polymer Physics* (Oxford University, New York, 2006).
[11] M. Lattuada, H. Wu, and M. Morbidelli, J. Colloid Interface Sci. **268**, 96 (2003).
[12] G. M. Wang and C. M. Sorensen, Phys. Rev. E **60**, 3036 (1999).
[13] P. N. Pusey, J. G. Rarity, R. Klein, and D. A. Weitz, Phys. Rev. Lett. **59**, 2122 (1987).
[14] H. M. Lindsay, R. Klein, D. A. Weitz, M. Y. Lin, and P. Meakin, Phys. Rev. A **38**, 2614 (1988).
[15] M. Lattuada, H. Wu, and M. Morbidelli, Langmuir **20**, 5630 (2004).
[16] U. Kätzel, M. Vorbau, M. Stintz, T. Gottschalk-Gaudig, and H. Barthel, Part. Part. Syst. Charact. **25**, 19 (2008).
[17] P. Wiltzius, Phys. Rev. Lett. **58**, 710 (1987).
[18] W. van Saarloos, Physica A **147**, 280 (1987).
[19] P. Tandon and D. E. Rosner, Ind. Eng. Chem. Res. **34**, 3265 (1995).
[20] S. Veerapaneni and M. R. Wiesner, J. Colloid Interface Sci. **177**, 45 (1996).
[21] J. Riseman and J. G. Kirkwood, J. Chem. Phys. **18**, 512 (1950).
[22] Z. Y. Chen, P. Meakin, and J. M. Deutch, Phys. Rev. Lett. **59**, 2121 (1987).
[23] W. Hess, H. L. Frisch, and R. Klein, Z. Phys. B: Condens. Matter **64**, 65 (1986).
[24] S. N. Rogak and R. C. Flagan, J. Colloid Interface Sci. **134**, 206 (1990).
[25] A. V. Filippov, J. Colloid Interface Sci. **229**, 184 (2000).
[26] A. Moskal and A. C. Payatakes, J. Aerosol Sci. **37**, 1081 (2006).
[27] D. M. Heyes, M. J. Nuevo, and J. J. Morales, Mol. Phys. **88**, 1503 (1996).
[28] D. M. Heyes, M. J. Nuevo, and J. J. Morales, J. Chem. Soc., Faraday Trans. **94**, 1625 (1998).
[29] D. M. Heyes, M. J. Nuevo, and J. J. Morales, Mol. Phys. **93**, 985 (1998).
[30] D. M. Heyes, M. J. Nuevo, J. J. Morales, and A. C. Branka, J. Phys.: Condens. Matter **10**, 10159 (1998).
[31] D. M. Heyes and A. C. Branka, Mol. Phys. **96**, 1757 (1999).
[32] R. Thouy and R. Jullien, J. Phys. A **27**, 2953 (1994).
[33] R. Thouy and R. Jullien, J. Phys. I **6**, 1365 (1996).
[34] D. Fry, A. Mohammad, A. Chakrabarti, and C. M. Sorensen, Langmuir **20**, 7871 (2004).
[35] See supplementary material at http://link.aps.org/supplemental/10.1103/PhysRevE.82.051402 for frequency distributions of the shape anisotropy parameters for fractal dimensions 2.1, 2.3, and 2.5.
[36] S. Plimpton, J. Comput. Phys. **117**, 1 (1995).
[37] http://lammps.sandia.gov/
[38] D. Frenkel and B. Smit, *Understanding Molecular Simulation: From Algorithms to Applications*, 2nd ed. (Academic Press, San Diego, 2002).
[39] J. M. Haile, *Molecular Dynamics Simulation: Elementary Methods* (John Wiley & Sons, New York, 1992).
[40] I. C. Yeh and G. Hummer, J. Phys. Chem. B **108**, 15873 (2004).
[41] B. Dünweg, J. Chem. Phys. **99**, 6977 (1993).
[42] M. Cappelezzo, C. A. Capellari, S. H. Pezzin, and L. A. F. Coelho, J. Chem. Phys. **126**, 224516 (2007).